RAA 2020 Vol. **20** No. **12**, 192(9pp) doi: 10.1088/1674-4527/20/12/192

http://www.raa-journal.org *http://iopscience.iop.org/raa*

***R**esearch in*
***A**stronomy and*
***A**strophysics*

Observational characteristics of SiO masers around VX Sgr

Jiang-Bo Su[1], Zhi-Qiang Shen[2], Xi Chen[3], Jing Liu[1], Yan Wang[1] and Yi-Bin Zhao[1]

[1] Department of Physics and Electronics, Yuncheng University, Yuncheng 044000, China; *sjb768@sohu.com*
[2] Shanghai Astronomical Observatory, Chinese Academy of Sciences, Shanghai 200030, China
[3] Center for Astrophysics, Guangzhou University, Guangzhou 510006, China

Received 2019 December 25; accepted 2020 May 28

Abstract SiO maser VLBA observations toward VX Sgr are performed at five epochs, and lots of maser spots are obtained. We make a statistical analysis on these spots. It is shown that the apparent sizes and the fluxes of maser spots decrease with increasing the distance from the central star. In addition, the similarity between the $v = 1$,2 (J=1–0) spectrums increases with epochs, consistent with the full width at half maximum (FWHM), while the total fluxes increase. The results may be related to the changeable pumping mechanisms.

Key words: masers — stars: individual (VX Sgr) — techniques: interferometric — turbulence

1 INTRODUCTION

SiO masers are often excited in the area between the photosphere and the dust shell (Elitzur 1992). Due to the compact and bright SiO maser spots, they can be used to investigate this region as a good probe. The radiative and collisional pumping mechanisms have been proposed (Elitzur 1980), but the dominant mechanisms still remain controversial. In the radiative pumping scheme, the energy requirements in $v = 1$, 2 (J=1–0) vibrational states are different (Bujarrabal et al. 1996), so the two masers can be excited in different regions, and the $v = 2$ masers should be closer to the central star. In the collisional pumping scheme, the two masers can occur in the same region (Lockett & Elitzur 1992). Therefore, the extent of spatial overlap between masers in these two vibrational states is important on constraining pumping mechanisms.

Many very long baseline interferometry (VLBI) observations have been performed toward a lot of late-type stars, and the relative positions of $v = 1$, 2 (J=1–0) SiO masers have also been obtained. Miyoshi et al. (1994) presented the spatial overlap between $v = 1$, 2 (J=1–0) masers in favor of collisional pumping. Desmurs et al. (2000) performed higher resolution observations using Very Large Baseline Array (VLBA) and reported that masers in the two transitions are separated by 1–2 mas in favor of radiative pumping. Soria-Ruiz et al. (2004) performed $v = 1$, 2 (J=1–0, J=2–1) SiO maser observations and found the line overlap could explain the results. Yi et al. (2005) found a spatial overlap between some maser spots with a smaller average radius of the $v = 2$ maser ring, which argued against the pure radiative pumping. Matsumoto et al. (2008) presented separations less than 0.5 mas for 42%–50% of maser pairs arguing for line overlap or collisional pumping. Kamohara et al. (2010) reported rare coincidences between the two masers, although with similar distributions, in support of radiative pumping mechanisms including line overlap effects. Su et al. (2012) concluded that the pumping mechanisms may be changeable based on observations at five epochs. Richter et al. (2013) reported a similar morphology between the two masers in the northeastern region of the envelope in favor of local collisional pumping. Yoon et al. (2018) found that the $v = 1$, (J=3–2) maser ring size reaches its maximum around the optical maximum implying the masers are mainly excited by radiative pumping. Oyadomari et al. (2018) found that the distribution of SiO $v = 2$,3 (J=1–0) masers around T Cep correlate well with each other in position, suggesting the mechanism of line overlapping may work. In this literature, three pieces of research presented observational results in favor of radiative pumping mechanisms, the others mainly supported collisional pumping or overlap. Given that the collisions with H_2 molecules provide energy for masers in the collisional scheme, more observations with short time intervals in future may be needed to investigate the relation between maser excitations and kinematics, and may be conducive to the understanding of pumping mechanisms.

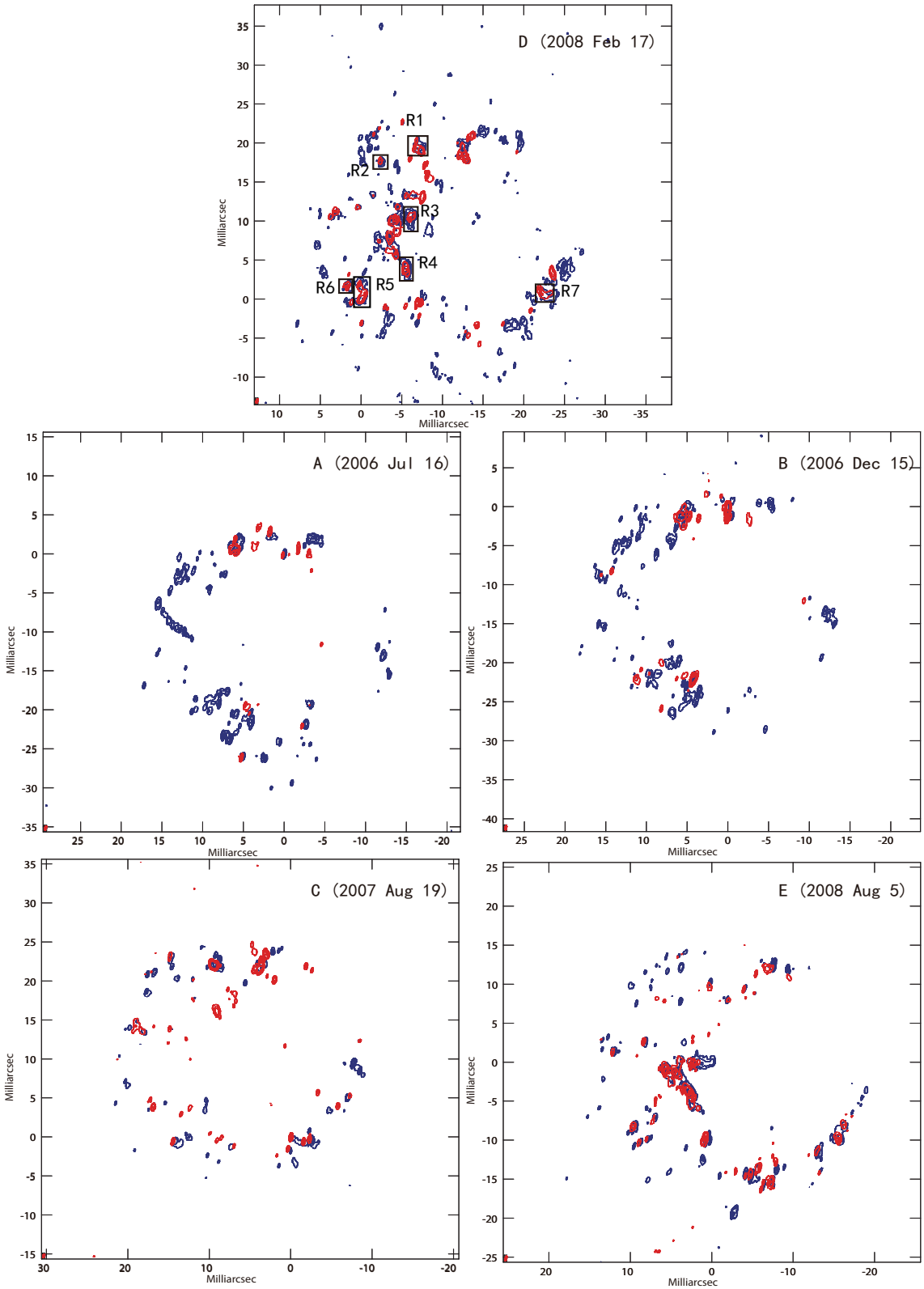

Fig. 1 Total intensity map at five epochs. The blue and red colors represent $v = 1$ and $v = 2$ (J=1–0) masers, respectively. The rms noise levels of $v = 1$ maser maps are 0.41, 0.47, 1.11, 0.44 and 0.87 Jy beam^{-1}. The rms noise levels of the other maser maps are 0.35, 0.26, 0.46, 0.73 and 1.30 Jy beam^{-1}, respectively. The contour levels equal the noise level multiplied by 1, 4 and 16.

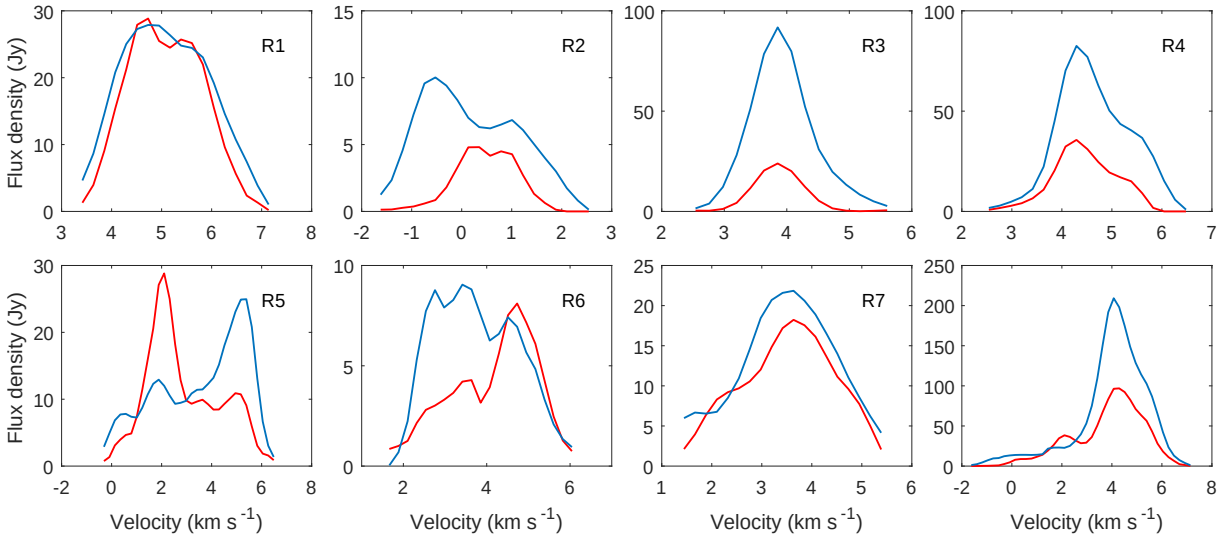

Fig. 2 Spectrums of maser spots in regions 1 to 7, which are marked in panel D of Fig. 1. The $v = 1$ and $v = 2$ (J=1–0) maser spectrums are represented by blue and red lines respectively. The lower right panel shows the spectrums obtained by summing the spectrums of regions 1 to 7.

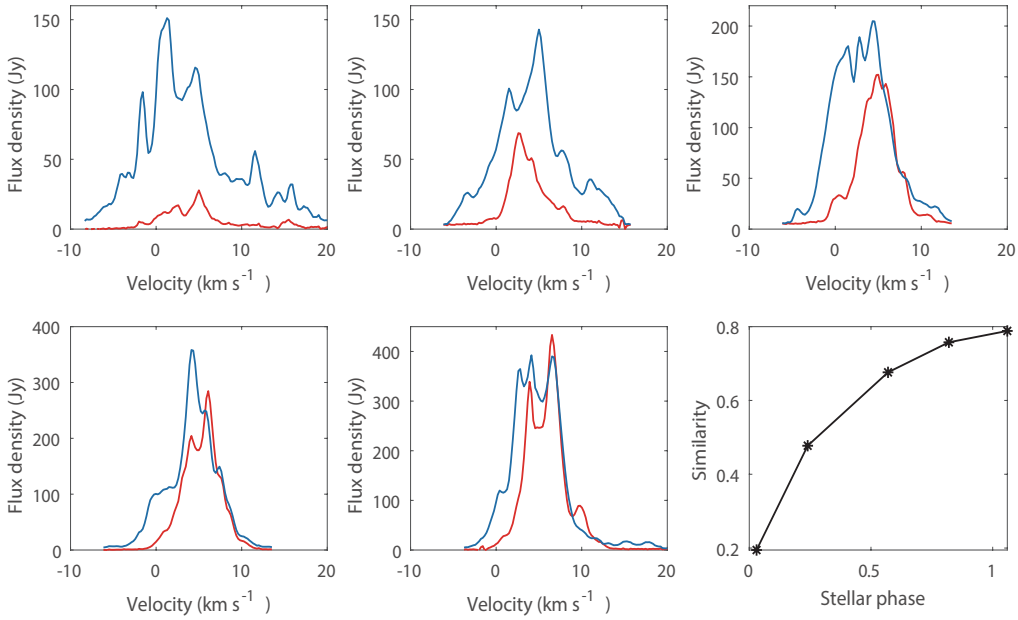

Fig. 3 Total power spectrums of $v = 1$, 2 (J=1–0) masers at five epochs, which are represented by blue and red lines respectively. They are obtained from the MK antenna. The lower right panel shows the similarity between spectrums of the two transitions.

VX Sgr is a M-type semi-regular variable with a period of 732 days (Kholopov et al. 1987) and a measured distance of 0.3-1.8 kpc (Humphreys et al. 1972; Pourbaix et al. 2003; Murakawa et al. 2003). As a late-type star with a photospheric radius of 4.41 mas (Chiavassa et al. 2010), VX Sgr loses mass at a rate of $1.3\times10^{-5}\ M_{\odot}$ (Knapp et al. 1989) and forms a dust shell, whose inner radius and thickness is about 60 mas and 30 mas, respectively (Danchi et al. 1994; Schuster et al. 2006). Between the dust shell and photosphere SiO masers appear. Kamohara et al. (2005) reported a SiO maser flux decrease around 1994, which may result from the diminished mass-loss. Chen et al. (2006) reported inward motions of the SiO masers based on the observations during 1999. The outward motions were also found based

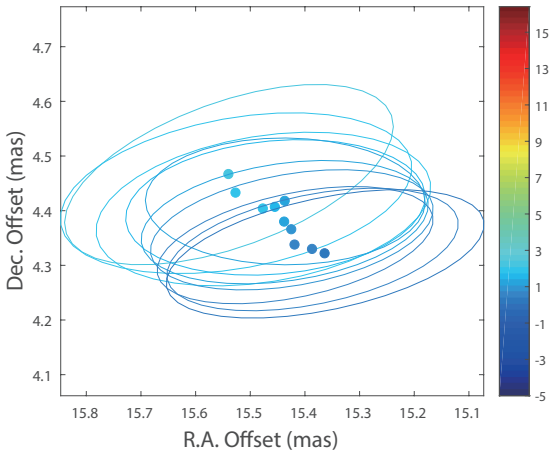

Fig. 4 One typical maser spot consisting of maser features, which are represented by several ellipses. The intensity peak positions of maser features are marked with solid dots. The color denotes the LOS velocity in units of km s^{-1}.

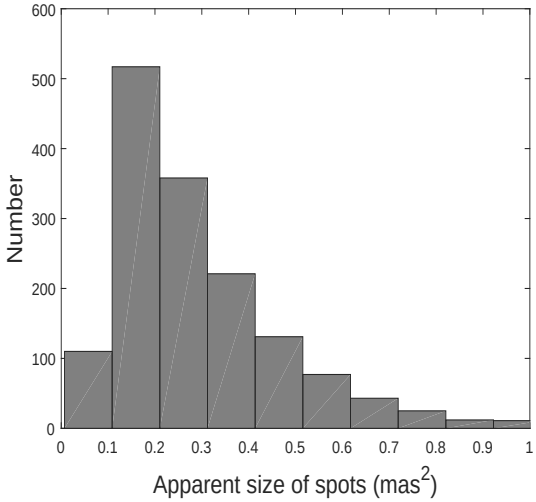

Fig. 5 Distributions of maser spot sizes.

on the observations at five epochs from 2006 Jul to 2008 Aug (Su et al. 2018).

In this paper, we describe the statistical characteristics of maser spots and try to explore the reason behind these phenomenons. The observations and data reduction are described in Section 2. In Section 3, we discuss the similarity of $v = 1, 2$ (J=1–0) maser spectrums, apparent sizes, velocity dispersions, full width at half maximum (FWHM), and flux densities. In Section 4, a summary is provided.

2 OBSERVATIONS AND DATA REDUCTION

We performed VLBA observations of SiO masers ($v = 1$, $v = 2$, J=1–0) toward VX Sgr at five epochs, which covered one complete cycle with an interval of ∼6 months. The data reduction was conducted using Astronomical Image Processing System (AIPS). The template spectrum method was used to calibrate the amplitude. A compact and bright maser spot was selected as a phase reference source, then the positions of all maser spots relative to this source could be obtained using a phase reference technology. The SiO masers present a ring structure except for $v = 2$ masers at the first two epochs. At the last two epochs, many bright maser spots in the two transitions appear and show almost the same shape and location. The details of the data reduction and results have been described by our previous work (Su et al. 2012).

3 DISCUSSION

3.1 Similarity between $v = 1$ and $v = 2$ (J=1–0) Maser Spectrums

SiO masers are located at ∼3 stellar radii from the central star (Chen et al. 2006). Maser observations show complex kinematics in this region due to shock waves, stellar pulsations, and gravity (Chen et al. 2006, Assaf et al. 2011). Since a single SiO maser spot originates from a small clump of moving gas, its spectrum is characterized by the velocity along the line of sight (LOS), turbulence in the gas clump, and the intensity. If the $v = 1, 2$ (J=1–0) maser spots are both excited in the same clump of gas (i.e., at the same position), they should have similar characteristics. So the two types of maser spots should have similar spectrums. If the $v = 1, 2$ (J=1–0) maser spots are generated in different gas clumps (i.e., at different positions), they tend to have different characteristics due to the complexity of atmospheric motions around the central star. So the spectrums of the two maser spots should be dissimilar. Therefore, if SiO masers in the two transitions are generated at the same positions, the total power spectrums obtained by a single antenna should be similar. Otherwise, they are dissimilar. As a result, the relative positions of the two masers can be indirectly reflected by comparing their total power spectrums. Then we use the VLBA observation in February 2008 to further illustrate this method. Panel D of Figure 1 presents the total intensity map, where seven regions are marked with rectangles. In regions 1 to 7, the $v = 1, 2$ (J=1–0) maser spots are overlapped with similar contours, so they can be considered to occur in the same regions. Their spectrums are obtained using AIPS tasks TVWIN and IMEAN and

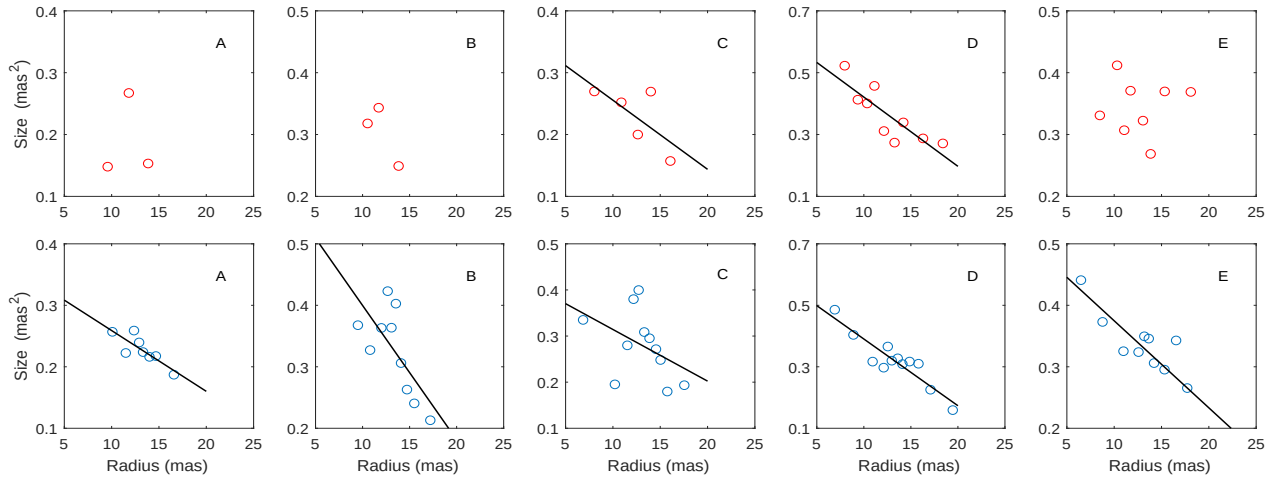

Fig. 6 Correlations between maser apparent sizes and distances from the central star. Upper panels: $v = 2$ masers; lower panels: $v = 1$ masers.

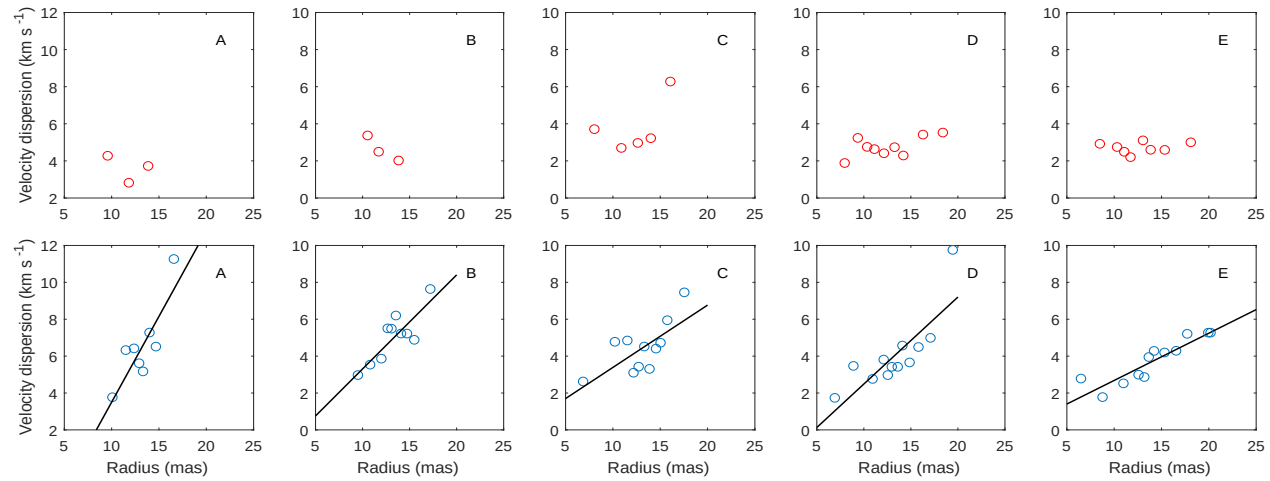

Fig. 7 Correlations between LOS velocity dispersions and distances from the central star. *Upper panels*: $v = 2$ masers; *Lower panels*: $v = 1$ masers.

plotted in Figure 2. It can be found that the spectrums of the two masers tend to be similar in the same region. To make a quantitative study, we describe the similarity using the formula:

$$S = 1 - \sum_{i=1}^{n} \left[\left| \frac{y_{1i} - y_{2i}}{y_{1i} + y_{2i}} \right| \times \frac{y_{1i} + y_{2i}}{\sum_{i=1}^{n} (y_{1i} + y_{2i})} \right] \quad (1)$$

where n is the number of spectral channels, y_{1i} and y_{2i} denote the flux densities of $v = 1$ and $v = 2$ maser features obtained from the i-th spectral channel. The absolute value denotes the similarity between y_{i1} and y_{2i}. Since both y_{1i} and y_{2i} are positive, their similarity falls between 0 and 1. Given that the similarities of maser spots at different positions should be comparable and have the same range of values, the similarity between y_{1i} and y_{2i} needs to be averaged. Moreover, given that the channels with higher flux densities are more important, a flux-weighted average is used. The right side of the multiplication sign in the formula is the weight, and the function S reflects the similarity. The bigger the value, the more similar the v = 1,2 maser spectrums. According to this formula, the similarity between spectrums for regions 1 to 7 can be calculated to be 0.91, 0.5, 0.35, 0.55, 0.7, 0.75, and 0.88 respectively. The spectrums of these seven pairs of maser spots are summed according to the corresponding velocities, the result is shown in the lower right panel of Figure 2. The similarity is 0.69. The big value suggests

these seven pairs of maser spots occur in the same regions, which is consistent with the total intensity map.

We performed VLBA observations of $v = 1, 2$ (J=1–0) SiO masers around VX Sgr from 2006 to 2008. Figure 3 shows the total power spectrums at five epochs, which are obtained from the Mauna Kea (MK) antenna. The blue and red lines represent $v = 1$ and $v = 2$ masers, respectively. According to formula 1, we calculate the similarity between the total power spectrums, and the results are presented in the lower right panel of Figure 3. It can be seen that the similarity gradually increases from 0.19 to 0.79, suggesting that the spatial distributions of the two masers become more and more similar.

To confirm this result, we identify $v = 1, 2$ maser pairs, which have angular distances less than the typical size of maser spots (0.5 mas) and LOS velocity differences less than 0.22 km s^{-1} corresponding to one channel (Matsumoto et al. 2008). Such one maser pair can be considered to originate from the same gas clump. The total fluxes of these maser pairs at each epoch are 445.0, 209.2, 860.3, 3666.4, and 5540.4 Jy, the proportions of which to the total fluxes of all maser spots at each epoch are 11.1%, 6.6%, 12.2%, 43.7%, and 42.4%, respectively. The values roughly show an increasing trend and suggest the spatial distribution gradually becoming similar, which is consistent with the similarities between spectrums and consistent with the VLBA mapping results that spatial distributions of $v = 1, 2$ masers change from being dissimilar to being similar. The mapping results presented in Figure 1 show more spatial overlaps at the last two epochs than at the first three epochs. Usually, pumping mechanisms are investigated based on relative spatial distributions. The similar distributions are predicted by collisional pumping or line overlap, and the different distributions by radiative pumping. The different relative distributions at the first three epochs suggest the radiative pumping, and the similar distributions at the last two epochs suggest the collisional or line overlap. Therefor, the dominant pumping mechanisms may change with time.

3.2 Apparent Sizes of Maser Spots

A maser spot originates from a clump of gas with a typical velocity range of $\sim$1 km s^{-1} (Chen & Shen 2008). Because of a spectral resolution of 0.22 km s^{-1}, the data of maser spots are recorded in several adjacent channels, and maser features are formed in each channel. We identify maser spots according to the criteria that maser features appear in at least three channels and are located within $\sim$ 0.5 mas. Figure 4 presents a typical maser spot with colors indicating LOS velocities. The spot consists of several features represented by ellipses, which are the results of

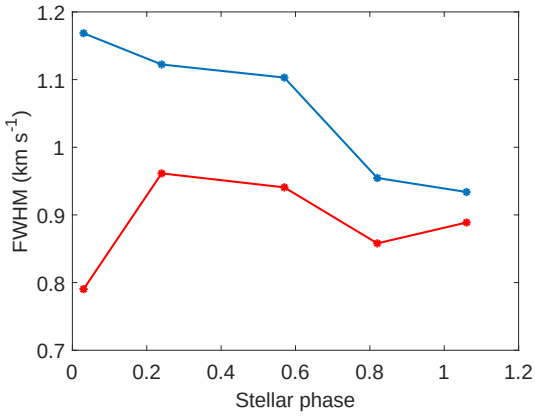

Fig. 8 Mean values of FWHM for $v = 1$ and $v = 2$ (J=1–0) maser spots, which are represented by blue and red lines respectively. The standard deviations for $v = 1$ masers are 0.59, 0.61, 0.54, 0.49 and 0.55 km s^{-1} respectively. For $v = 2$ masers, they are 0.44, 0.43, 0.46, 0.40 and 0.53 km s^{-1} respectively.

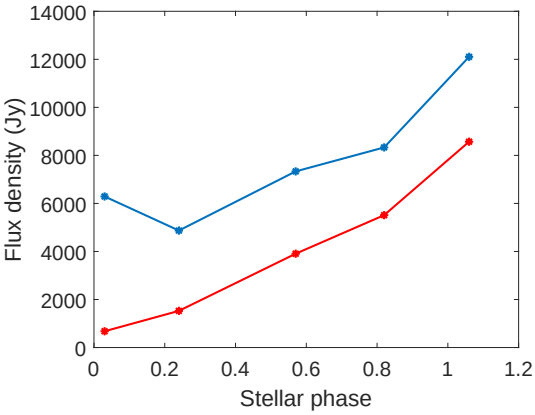

Fig. 9 Flux densities of $v = 1$ and $v = 2$ (J=1–0) masers represented by blue and red lines.

2D Gaussian fits using AIPS task SAD. The peak positions of maser features are marked with solid dots, which are aligned successively. The apparent size of one spot can be determined by calculating the total area surrounded by all ellipses. The histograms in Figure 5 show a distribution of apparent sizes of all maser spots. The number peaks between 0.1 and 0.2 mas^2. However, the sizes of most of maser spots are equal or greater than 0.1 mas^2, which can result from the VLBA beam, $\sim$ 0.5 mas $\times$ 0.15 mas corresponding to an area of 0.06 mas^2. For the maser features smaller than the beam, their apparent sizes are broadened. In addition, the interstellar scattering is also responsible for the size broadening. In VLBI observations of SiO masers, almost a half of total flux observed by a single antenna is missed. A recent study shows that the missing flux is mainly contained in the weak spots at the noise level (Desmurs et al. 2018). These undetected maser spots may be very small.

Table 1 Parameters Obtained from a Linear Fit to Maser Apparent Sizes and Distances from the Central Star

Parameters	Epoch A	Epoch B	Epoch C	Epoch D	Epoch E
k,$v=1$	–0.010±0.007	–0.022±0.018	–0.011±0.017	–0.022±0.007	–0.014±0.006
b,$v=1$	0.358±0.088	0.618±0.246	0.426±0.230	0.607±0.090	0.516±0.078
coef,$v=1$	–0.83	–0.70	–0.44	–0.92	–0.89
k,$v=2$	...	...	–0.011±0.022	–0.022±0.013	...
b,$v=2$	...	...	0.367±0.274	0.645±0.168	...
coef,$v=2$	0.06	–0.81	–0.69	–0.84	0.04

The letters k and b represent the slope and intercept respectively. For $v=2$ masers at epoch A, B and E, the linear fit is not made because of the lack of linear correlations.The coef represents the correlation coefficient.

Table 2 Parameters Obtained from a Linear Fit to LOS Velocity Dispersions and Distances from a Central Star

Parameters	Epoch A	Epoch B	Epoch C	Epoch D	Epoch E
k,$v=1$	0.930±0.582	0.510±0.262	0.338±0.254	0.472±0.237	0.256±0.100
b,$v=1$	–5.799±7.784	–1.792±3.546	0.010±3.401	–2.228±3.251	0.122±1.419
coef,$v=1$	0.79	0.85	0.65	0.73	0.93

The slope, intercept and correlation coefficient are represented by k, b and coef, respectively. For the same reason mentioned in Table 1, the linear fit is only made for $v=1$ masers.

Table 3 Parameters Obtained from a Linear Fit to Fluxes and Distances from the Central Star

Parameters	Epoch A	Epoch B	Epoch C	Epoch D	Epoch E
k,$v=1$	–0.943±4.1930	–1.257±1.436	...	–3.58±2.182	–5.7±3.038
b,$v=1$	35.580±56.050	28.350±19.440	...	66.890±29.960	109.500±43.050
coef,$v=1$	–0.22	–0.58	0.03	–0.76	–0.82
k,$v=2$	...	...	...	–2.952±2.221	–5.771±5.509
b,$v=2$	...	...	...	59.210±28.910	112.200±72.220
coef,$v=2$	0.73	–0.91	–0.32	–0.77	–0.72

The slope, intercept and correlation coefficient are represented by k, b and coef, respectively.

As shown in Figure 1, the maser spots are distributed in a ring-like structure, the center of which is obtained by fitting a simple circle model for each epoch. Around the center, a series of annuluses with different inner and outer radii can also be obtained. By calculating the mean sizes of maser spots in an annulus, we investigate the correlation between maser apparent sizes and radii. We assume that the apparent sizes $y_{\rm size}$ and radii $x_{\rm radii}$ satisfy the line equation:

$$y_{\rm size} = k \times x_{\rm radii} + b + f \qquad (2)$$

where f represents the fluctuation caused by unknown factors. By averaging the apparent sizes and radii of maser spots in an annulus, the fluctuation f tends to zero and the clear correlation between the apparent sizes and radii can be shown. By averaging twenty (or more) adjacent data points in an annulus, the upper and lower panels in Figure 6 show correlations for $v=2$ and $v=1$ maser spots, respectively. The $v=1$ maser data show clear correlations at five epochs. However, for $v=2$ maser, the clear correlation is only shown at the third and fourth epochs. The parameters from a linear fit are presented in Table 1. The high correlation coefficients for $v=2$ masers at the first two epochs cannot indicate high correlations, because of less data points. The negative slopes indicate that the apparent size of the maser spots decreases with the distance from the central star. In addition, the sizes of maser spots are correlated with fluxes, which also decrease with the distance from the central star (see Sect. 3.5 for a detailed discussion). It is natural that big maser spots have high fluxes.

3.3 Velocity Dispersions along the Line of Sight

The LOS velocity of maser spots varies around the systemic velocity, 5.3 km s^{-1} (Chapman & Cohen 1986). Like investigating the correlation between the apparent sizes of maser spots and the distances from the central star, the LOS velocity dispersions of maser spots in an annulus around the systemic velocity are also calculated based on the following formula:

$$\sqrt{\frac{\sum_{i=1}^{n}(v_i - 5.3)^2}{n-1}} \qquad (3)$$

where n is the number of maser spots in an annulus and v_i is the LOS velocity. The results are shown in Figure 7. The $v=2$ velocity dispersions mainly range from 2 to 4 km s^{-1}, which is generally smaller than $v=1$ velocity dispersions. Moreover, Figure 3 also shows smaller velocity ranges for $v=2$ masers indicating a more

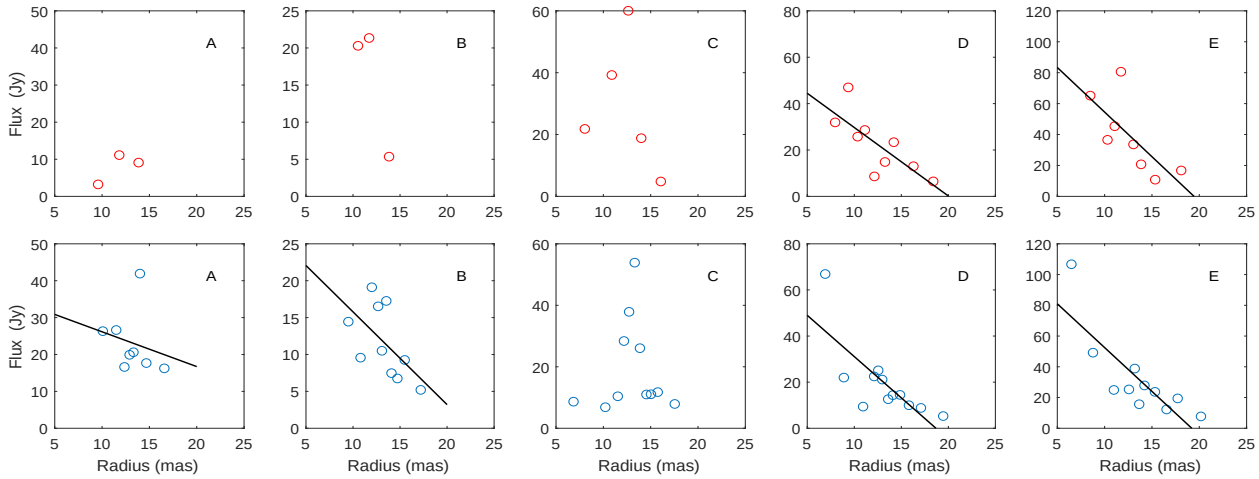

Fig. 10 Correlations between fluxes and distances from the central star. *Upper panels*: $v = 2$ masers; *lower panels*: $v = 1$ masers.

concentrated velocity distribution around the systemic velocity, which is consistent with its smaller velocity dispersions. The previous research reports an expanding maser shell (Su et al. 2018). In this case, the $v = 2$ LOS velocities closer to the systemic velocity and smaller velocity dispersions suggest that the $v = 2$ maser spots should be distributed in a narrower region close to the plane of the sky, compared with $v = 1$ maser spots. The interference is in agreement with that the $v = 2$ maser spots are excited in a narrower range of physical conditions (Gray & Humphreys 2000).

The velocity dispersions, which are calculated from $v = 1$ maser spots located between the dust formation region and the photosphere, increase with the radius. The fitted line parameters are listed in Table 2. In outer parts of the maser shell, the interaction of $v = 1$ maser spots with ambient gas clumps can lead to complex motions and greater velocity dispersions. For $v = 2$ maser spots, the increasing velocity dispersions with the radius are not found. At the first three epochs, only several data points are available. At the other two epochs, the velocity dispersions almost do not change with the radius. The results can be related to the inferred distribution closer to the plane of the sky. In this case, it is difficult to change the LOS velocity by the interaction with ambient gas clumps.

3.4 Full Width at Half Maximum

By performing a Gaussian fit to the velocities and flux densities of features contained in one maser spot, we can obtain the FWHM. Figure 8 shows the mean FWHM for $v = 1, 2$ masers at five epochs with a standard deviation of $\sim$0.4 km s^{-1}. The differences between the mean values are 0.38 , 0.16 , 0.16, 0.10 and 0.05 km s^{-1} respectively, which changes from large to small. The changes suggest that the spectrums of masers spots are more and more similar, which is consistent with the trend of the similarity shown in Figure 3. In addition, we notice that the FWHM for $v = 1$ masers is larger than that for $v = 2$ masers. Given that the FWHM is related to the turbulence, the gas clumps excited $v = 1$ masers seem to be more turbulent.

3.5 Flux Densities

Figure 9 shows flux densities of $v = 1, 2$ (J=1–0) masers at five epochs, which is obtained from summing over flux densities for all channels shown in Figure 3. The flux densities of $v = 1$ masers are obviously larger than that of $v = 2$ masers. The $v = 1$ masers can be excited under a wider range of physical conditions (Gray & Humphreys 2000), which can result in more maser spots and then larger flux densities. Moreover, the flux densities of the two masers are on the increase. This trend does not correlate with the optical light curve shown in figure 4 in Su et al. (2012), arguing against purely radiative pumping. Lockett & Elitzur (1992) found that the collisional pumping mechanism can produce stronger masers. Combined with the overlapping maser spots at the last two epochs (Su et al. 2012), the increase of flux densities may result from collisional pumping that gradually becomes dominant.

Figure 10 shows the correlations between the fluxes of maser spots and the distances from the central star. Table 3 presents the parameters from linear fitting. The upper panels at the first and second epochs show less data points, so there are not clear correlations even though

the absolute values of the correlation coefficients are high (0.73 and -0.91 for $v = 2$ masers at the first two epochs, respectively). The two panels for $v = 1, 2$ masers at the third epoch do not show clear correlations, which can be related to some unknown factors. More observations can be needed to further investigate the reason. In the other panels, the fluxes of maser spots decrease with the distance from the central star, which may be related to energy sources. In the region close to the central star, the sufficient energy can be provided to excite maser spots with high fluxes.

4 CONCLUSIONS

We made a statistical analysis on the $v = 1, 2$ (J=1–0) masers and provided possible explanations. The main conclusions are the following. (1) The similarity between $v = 1, 2$ maser spectrums can reflect the extent of the spatial overlap. During our observations, the similarity gradually changes from 0.19 to 0.79, suggesting the masers in the two transitions gradually tend to occur in the same region. The results may be caused by the changeable pumping mechanisms. (2) The apparent sizes of maser spots generally decrease with the distance from the central star, which is consistent with the decreasing fluxes. (3) Compared with $v = 1$ maser spots, the LOS velocity dispersions of $v = 2$ maser spots are smaller, which indicates the $v = 2$ velocities are closer to the systemic velocity and may imply their distribution is closer to the plane of the sky. (4) The difference between the mean values of FWHM for the two transitions gradually becomes small, which is in agreement with the similarity. The FWHM of $v = 1$ maser spots is larger than the other suggesting that the $v = 1$ maser spots may originate in more turbulent regions. (5) The fluxes in the two transitions are on the increase and do not correlate with the optical light curve, arguing against pure radiative pumping.

Acknowledgements This work is supported by the National Natural Science Foundation of China (Grant Nos. U1431125 and U1631106), the Science and Technology Innovation Program of Shanxi Province (2019L0876) and Yuncheng University (YQ-2019016).

References

Assaf, K. A., Diamond, P. J., Richards, A. M. S., & Gray, M. D. 2011, MNRAS, 415, 1083
Bujarrabal, V., Alcolea, J., Sanchez Contreras, C., & Colomer, F. 1996, A&A, 314, 883
Chapman, J. M., & Cohen, R. J. 1986, MNRAS, 220, 513
Chen, X., & Shen, Z.-Q. 2008, ApJ, 681, 1574
Chen, X., Shen, Z.-Q., Imai, H., & Kamohara, R. 2006, ApJ, 640, 982
Chiavassa, A., Lacour, S., Millour, F., et al. 2010, A&A, 511, A51
Danchi, W. C., Bester, M., Degiacomi, C. G., Greenhill, L. J., & Townes, C. H. 1994, AJ, 107, 1469
Desmurs, J. F., Alcolea, J., Bujarrabal, V., Colomer, F., & Soria-Ruiz, R. 2018, in IAU Symposium, 336, Astrophysical Masers: Unlocking the Mysteries of the Universe, eds. A. Tarchi, M. J. Reid, & P. Castangia, 387
Desmurs, J. F., Bujarrabal, V., Colomer, F., & Alcolea, J. 2000, A&A, 360, 189
Elitzur, M. 1980, ApJ, 240, 553
Elitzur, M. 1992, ARA&A, 30, 75
Gray, M. D., & Humphreys, E. M. L. 2000, New Astron., 5, 155
Humphreys, R. M., Strecker, D. W., & Ney, E. P. 1972, ApJ, 172, 75
Kamohara, R., Deguchi, S., Miyoshi, M., & Shen, Z.-Q. 2005, PASJ, 57, 341
Kamohara, R., Bujarrabal, V., Honma, M., et al. 2010, A&A, 510, A69
Kholopov, P. N., Samus', N. N., Kazarovets, E. V., & Kireeva, N. N. 1987, Information Bulletin on Variable Stars, 3058, 1
Knapp, G. R., Sutin, B. M., Phillips, T. G., et al. 1989, ApJ, 336, 822
Lockett, P., & Elitzur, M. 1992, ApJ, 399, 704
Matsumoto, N., Omodaka, T., Imai, H., et al. 2008, PASJ, 60, 1039
Miyoshi, M., Matsumoto, K., Kameno, S., Takaba, H., & Lwata, T. 1994, Nature, 371, 395
Murakawa, K., Yates, J. A., Richards, A. M. S., & Cohen, R. J. 2003, MNRAS, 344, 1
Oyadomari, M., Imai, H., Nagayama, T., et al. 2018, PASJ, 70, 33
Pourbaix, D., Platais, I., Detournay, S., et al. 2003, A&A, 399, 1167
Richter, L., Kemball, A., & Jonas, J. 2013, MNRAS, 436, 1708
Schuster, M. T., Humphreys, R. M., & Marengo, M. 2006, AJ, 131, 603
Soria-Ruiz, R., Alcolea, J., Colomer, F., et al. 2004, A&A, 426, 131
Su, J. B., Shen, Z. Q., Chen, X., & Jiang, D. R. 2018, ApJ, 853, 42
Su, J. B., Shen, Z. Q., Chen, X., et al. 2012, ApJ, 754, 47
Yi, J., Booth, R. S., Conway, J. E., & Diamond, P. J. 2005, A&A, 432, 531
Yoon, D.-H., Cho, S.-H., Yun, Y., et al. 2018, Nature Communications, 9, 2534